Climate Dynamics (2023) 60:3695–3712
https://doi.org/10.1007/s00382-022-06534-4

Internal multi-centennial variability of the Atlantic Meridional Overturning Circulation simulated by EC-Earth3

Virna L. Meccia[1] · Ramón Fuentes-Franco[2,3] · Paolo Davini[4] · Katinka Bellomo[4,5] · Federico Fabiano[1] · Shuting Yang[6] · Jost von Hardenberg[4,5]

Received: 29 April 2022 / Accepted: 3 October 2022 / Published online: 21 October 2022

Abstract
We report a multi-centennial oscillation of the Atlantic Meridional Overturning Circulation (AMOC) simulated by the EC-Earth3 climate model under the pre-industrial climate. This oscillation has an amplitude of ~6 Sv and a period of ~150 years and significantly impacts the atmosphere. We find that it is a self-sustained low-frequency internal variability, driven by the accumulation of salinity anomalies in the Arctic and their release into the North Atlantic, affecting the water column stability and the deep convection. Sea ice plays a major role in creating the salinity anomaly in the Arctic, while the anomalous Arctic oceanic circulation, which drives the exchange of liquid freshwater between the Arctic and the open ocean, is the main responsible for its southward propagation. Interestingly, EC-Earth3 simulations with increased greenhouse concentrations, and therefore under a warmer climate, do not exhibit these strong AMOC fluctuations. We hypothesize that in a quasi-equilibrium climate with a global air surface temperature 4.5° higher than the pre-industrial period, the low amount of sea ice in the high latitudes of the North Atlantic is no longer able to trigger the mechanism.

Keywords AMOC · Multi-centennial variability · EC-Earth3 · Pre-industrial climate

1 Introduction

The Atlantic Meridional Overturning Circulation (AMOC) consists of an extensive system of ocean currents that contributes to the heat redistribution around the globe. It is constituted by a northward component of warm and salty waters in the upper layers of the Atlantic, the Gulf Stream, and a southward component of cold waters in the deep layers, the North Atlantic Deep Water (Buckley and Marshall 2016). The AMOC transports a substantial amount of heat from the south, including the Southern Hemisphere and the Tropics, toward the North Atlantic (Bryan 1962; Ganachaud and Wunsch 2000; Jackson et al. 2015; Weijer et al. 2020), with considerable implications on the global climate. Indeed, paleoclimate records suggest that past abrupt climate changes were a response to changes in the AMOC (Broecker et al. 1985; Rahmstorf 2002; Clark et al. 2002; McManus et al. 2004; Liu et al. 2009). Moreover, the AMOC variability on the centennial timescale is thought to play a role in masking some of the anthropogenic effects of climate change over the coming years (Bonnet et al. 2021; Latif et al. 2022). Therefore, understanding the AMOC behaviour and the mechanisms associated with its natural variability is necessary to assess the climate response to anthropogenic forcing and climate projections.

The systematic monitoring of the AMOC started in 2004 with the RAPID array across the Atlantic at 26.5° N (Cunningham et al. 2007). Although it provides direct information on the AMOC strength, the observational record is relatively short. Caesar et al. (2021) compared various proxy records to reconstruct the AMOC evolution of the

✉ Virna L. Meccia
v.meccia@isac.cnr.it

1 National Research Council of Italy, Institute of Atmospheric Sciences and Climate, Bologna, Italy

2 Rossby Centre, Swedish Meteorological and Hydrological Institute, Norrköping, Sweden

3 Bolin Centre for Climate Research, Stockholm University, Stockholm, Sweden

4 National Research Council of Italy, Institute of Atmospheric Sciences and Climate, Turin, Italy

5 Department of Environment, Land and Infrastructure Engineering, Polytechnic University of Turin, Turin, Italy

6 Danish Meteorological Institute, Copenhagen, Denmark

last 1500 years, but they focused on the AMOC decline of the mid-twentieth century. There is evidence of fluctuations of the AMOC on different timescales, from inter-annual to multi-centennial. The driving mechanisms proposed in the literature depend on the timescale of the oscillations. Many studies show that the wind-driven variability mainly explains the seasonal to inter-annual AMOC fluctuations (Kanzow et al. 2010; Xu et al. 2014; Zhao and Johns 2014; Yang 2015), with a minor contribution being explained by the intrinsic ocean variability (Grégorio et al. 2015). On decadal and multi-decadal timescales, the AMOC variability is often described by a delayed response to the North Atlantic Oscillation (NAO; Latif et al. 2006). The NAO is associated with variations in the storm tracks over the North Atlantic (Gerber and Vallis 2009), which affect the large-scale atmospheric circulation and the precipitation and temperature anomalies. These changes in heat flux and wind stress associated with the NAO result in buoyancy changes in the western sub-polar North Atlantic that force decadal AMOC fluctuations (Böning et al. 2006; Deshayes and Frankignoul 2008; Xu et al. 2013; Danabasoglu et al. 2016). At the same time, and through the poleward ocean heat transport, the fluctuations in the ocean circulation might force anomalies of sea surface temperature (SST) patterns to reverse the NAO phase (Årthun et al. 2021). On the other hand, AMOC variability in this timescale is also thought to be a driver of Atlantic Multi-decadal Variability (AMV; Bjerknes 1964; Knight et al. 2005; Zhang et al. 2007; Msadek and Frankignoul 2009; McCarthy et al. 2015). The AMV is manifested as a basin-scale SST and sea level pressure anomaly in the North Atlantic, with implications for the Northern Hemisphere (Steinman et al. 2015) and European (Sutton and Dong 2012) climates.

However, the centennial to multi-centennial variability of the AMOC is less studied. Some studies with numerical models found these low-frequency oscillations, although both the frequency of the fluctuations and the mechanism proposed for this variability are model dependent. For instance, one of the mechanisms proposed for the centennial and multi-centennial variability is related to density anomalies propagating from the Southern Ocean into the North Atlantic sub-polar gyre, affecting the stability of the water column in the deep-water formation sites. Indeed, among other studies, Mikolajewicz and Maier-Reimer (1990) found natural ocean variability in response to a simulated white-noise atmospheric forcing in an ocean general circulation model. These fluctuations have a period of roughly 320 years, and the signal is strongest in the Southern Ocean, which then is propagated to the North Atlantic. Delworth and Zeng (2012) found variations of the AMOC with a timescale of 200–500 years in the GFDL-CM2.1 climate model. In that model, salinity anomalies propagate from the Southern Ocean to the convective locations of the North Atlantic high latitudes. Martin et al. (2013) also found multi-centennial variability in the AMOC as a response to a signal originated in the Southern Ocean in the Kiel Climate Model, a coupled atmosphere–ocean-sea ice general circulation model.

A second mechanism proposed for sustaining the centennial and multi-centennial variability of the AMOC is related to salinity anomalies propagating from the tropics and subtropics into the North Atlantic sub-polar gyre. Vellinga and Wu (2004) identified a centennial mode of AMOC variability in the HadCM3 coupled model driven by air-sea interaction in the Atlantic. They found that a strong phase of the AMOC implies a strong northward ocean heat transport causing an anomaly of the cross-equatorial SST gradient. Consequently, the Inter-Tropical Convergence Zone (ITCZ) shifts to the north, releasing an extra freshwater flux in the tropical North Atlantic and causing a negative salinity anomaly. This anomaly propagates into the sub-polar gyre in around 5–6 decades, inhibiting the deep-water formation and causing a slow-down of the AMOC. Then, the opposite phase of the mechanisms starts. Menary et al. (2012) tested the mechanism proposed by Vellinga and Wu (2004) in two other climate models: the Kiel Climate Model showed elements of this mechanism, whereas the MPI-ESM did not. In particular, the latter reproduced a weaker cross-equatorial SST gradient, which they attributed to a stronger mean AMOC than the one simulated by the other two models.

A third mechanism proposed in the literature to explain the multi-centennial variability of the AMOC consists of density variations generated in the Arctic Ocean that propagate into the North Atlantic. Jiang et al. (2021) found multi-centennial AMOC fluctuations in the IPSL-CM6-LR climate model. These fluctuations are sustained by the oceanic freshwater exchange between the North Atlantic and the Arctic, with little atmospheric influence. A similar mechanism in which oscillations of the AMOC are maintained by an interplay between the central Arctic and the Nordic seas was previously found by Jungclaus et al. (2005) in the coupled ECHAM5/MPI-OM model but with a multi-decadal timescale. Also, Hawkins and Sutton (2007) found multi-decadal variability in the HadCM3, fed by salinity anomalies transported from the Arctic into the Nordic seas.

Reporting and understanding the low-frequency variability of the AMOC in an Earth System Model is of interest not only for the climate impacts but also to help better distinguish between forced and internal variability in long simulations. This paper aims to (a) document a multi-centennial AMOC variability in pre-industrial simulations of the EC-Earth3 climate model, (b) understand the mechanism behind the low-frequency variability in this specific model, and (c) investigate if this multi-centennial internal variability would also be present in a warmer climate. The following section describes the EC-Earth model, the simulations analysed, and the methods used. Section 3 introduces the multi-centennial

variability present in the pre-industrial runs. A mechanism behind the oscillation is proposed in Sect. 3.1, and the question of what happens in a warmer climate is addressed in Sect. 3.2. Section 4 is dedicated to conclusions.

2 Model simulations and methods

2.1 The climate model

The model used is the CMIP6-generation General Circulation Model (GCM) EC-Earth version 3 (Döscher et al. 2022). The atmospheric component consists of a modified cycle 36r4 Integrated Forecast System (IFS; ECMWF 2010) and includes the land-surface scheme H-TESSEL (Balsamo et al. 2009). The ocean model consists of the Nucleus for European Modelling of the Ocean (NEMO; Madec 2008) version 3.6, including the Louvain la Neuve (LIM3; Vancoppenolle et al. 2012) sea-ice model. The OASIS3-MCT (Valcke 2013) coupler version 3.0 exchanges fields between the atmosphere and ocean components. The IFS spatial resolution is T255L91, corresponding to a horizontal resolution of about 80 km and 91 vertical levels represented in a hybrid coordinate system. The model configuration in NEMO is the ORCA1L75, a tripolar grid with an average horizontal resolution of $1° \times 1°$ and 75 vertical levels.

To report the multi-centennial AMOC variability and to study the sustaining mechanism behind it, we analyse a 1000-year-long pre-industrial run (*piControl*, ensemble member r5i1p1f1) which follows the boundary conditions from the Coupled Model Intercomparison Project—Phase 6 protocol (Eyring et al. 2016). This simulation started after the spin-up and was run with fixed conditions representative of a pre-industrial climate (namely, using forcing from the year 1850). This way, we can evaluate the internal variability because the radiative forcing remains constant. We also looked at a set of 500-year-long simulations with fixed external forcing presented in Fabiano et al. (in preparation). These are branched off from the EC-Earth3 historical + SSP5-8.5 simulation in 1990, 2025, 2050 and 2100 (named '*b990*', '*b025*', '*b050*' and '*b100*'), with the greenhouse gases and aerosols kept fixed at the initial year's condition.

2.2 Methods

The AMOC index is defined here as the maximum Atlantic meridional streamfunction between 30° N and 50° N in the depth range of 500 m and 2000 m. Because we are interested in centennial to multi-centennial timescale, the high-frequency variability is filtered with a low-pass filter and cut-off period of 30 years. The regressed fields on the AMOC index are computed by a unit of change of the AMOC index, and consequently, they have units of the regressed field times Sv^{-1}.

We define three regions for assessing some of the diagnostics: the Labrador Sea (Labrador; 70° W–40° W, 45° N–72° N, see Fig. 3b), the Greenland-Iceland-Norwegian seas (GIN; 20° W–20° E, 65° N–82° N, see Fig. 3b), and the Arctic Sea (Arctic; northward of 78° N). The computation of density fields and the temperature and salinity contributions to the density changes were made offline through the computationally-efficient expression for the density using the TEOS-10 standard (Roquet et al. 2015). The annual means of 3D prognostic temperature and salinity fields were used for the computation.

The liquid and solid freshwater transports into the Arctic were computed according to Fuentes-Franco and Koenigk (2019). Both liquid and solid freshwater transports were calculated through the Fram Strait, Northern Baffin Bay, the Barents Sea and the Bering Strait (see Fig. 5b for details). The native grids of the model are used to get the gridline (line along the native grid) closest to the land points that define each strait. Then, the velocity fields perpendicular to the gridline are used: the 3D ocean velocity *vo* for the liquid freshwater transports and the 2D sea-ice velocity *siv* for the solid ones. The liquid freshwater transport in $m^3\ s^{-1}$ is estimated as:

$$fwt_{liquid} = \int_{p1}^{p2}\int_{D}^{\eta} \frac{(S_{ref} - S)}{S_{ref}} v dz dx$$

where S is the 3D *so* field in practical salinity units (psu), and v is the *vo* velocity perpendicular to the section in $m\ s^{-1}$. As in Aagaard and Carmack (1989), we use the value of 34.8 psu for the reference salinity *Sref*. The vertical integral goes from the bottom (D) to the surface (η), and the horizontal integration is along the length between the two land points that define the strait (*p1* and *p2*). Similarly, solid freshwater transport (i.e. the freshwater transport due to sea-ice drift) is computed as:

$$fwt_{solid} = \int_{p1}^{p2} \frac{(S_{ref} - S_{ice})}{S_{ref}} \frac{C_{ice}}{100} \frac{\rho_{ice}}{\rho_{water}} h_{ice} v_{ice} dx$$

where C_{ice} is the sea-ice concentration (*siconc*), h_{ice} is the sea-ice thickness (*sithick*) and v_{ice} is the sea-ice velocity perpendicular to the grid lines (*siv*). We assume ice salinity S_{ice} of 4 psu and density ρ_{ice} of 900 kg m^{-3} as in Serreze et al. (2006), and ρ_{water} of 1000 kg m^{-3}. The freshwater transports are computed from monthly data before computing the annual mean.

The significance of the lagged regressions and the regressed fields on the AMOC index is computed with the block bootstrapping technique. The blocks are determined by the autocorrelation e-folding decay time of the filtered

AMOC index, which is 25 years, and 1000 (for the lagged regressions) or 500 (for the regressed fields on the AMOC index) bootstrap samples were used. The significance is plotted for the 95% of confidence level.

3 Results

The 1000-year time-series and power spectral density of the AMOC index and the Atlantic meridional streamfunction regressed on the AMOC index are plotted in Fig. 1. The AMOC in the *piControl* run with EC-Earth3 is dominated by a fluctuation of about 150 years (Fig. 1c). The amplitude of these oscillations (black line in Fig. 1a) is larger than the amplitude of the inter-annual to multi-decadal variability (grey line in Fig. 1a). Indeed, the standard deviation of the low-frequency (period > 30 years) AMOC index is 1.77 Sv, and the standard deviation of the high-frequency variability (period < 30 years) is 0.76 Sv. This centennial to multi-centennial oscillation involves the whole Atlantic basin (Fig. 1b); the highest values of meridional streamfunction regressed on the AMOC index are between 30° N and 50° N at around 1000 m depth, in agreement with the AMOC index definition (Sect. 2).

The ocean sets the boundary conditions to the atmosphere through the sea surface temperature. Therefore, the oceanic

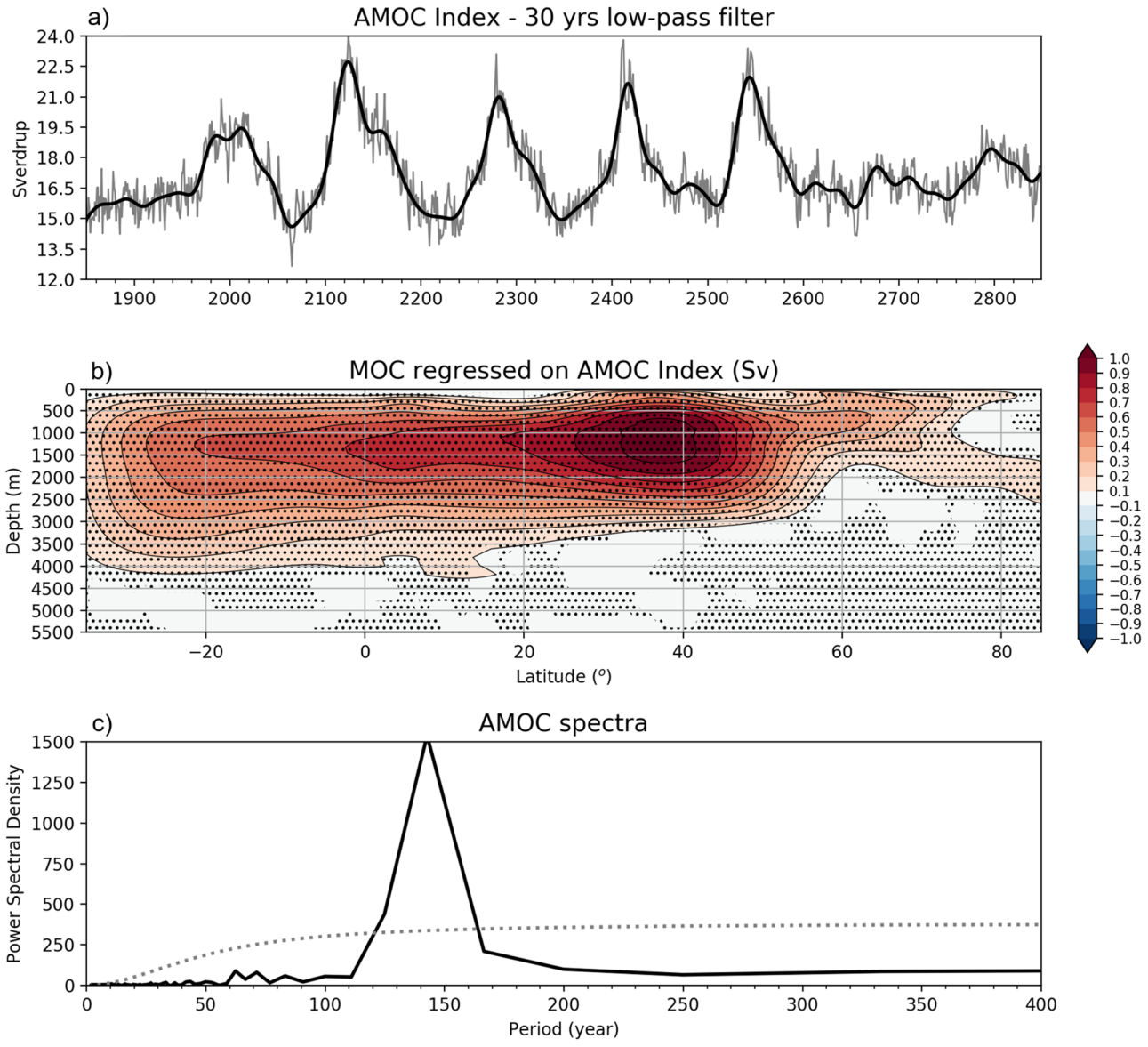

Fig. 1 **a** Time-series of annual AMOC index (grey) and low-frequency AMOC index (black). **b** Atlantic meridional streamfunction regressed on the AMOC index. **c** Power spectral density of the AMOC index. Significance at 95% confidence level in **b** and **c** are indicated by dots

low-frequency internal variability has implications for the atmosphere. To present an overview of the magnitude of these implications, we computed the composites of the winter and summer near-surface air temperature and precipitation for strong (coloured in red in Fig. 2a) and weak (coloured in blue in Fig. 2a) AMOC events. A strong or weak event is considered when the AMOC index exceeds or falls behind the mean value by one standard deviation. The differences between strong and weak events during the boreal winter (DJF) and summer (JJA) of the mean near-surface air temperature and precipitation fields are plotted in Fig. 2b, c and Fig. 2d, e, respectively. Because the AMOC is associated with northward heat transport, the near-surface air temperature is warmer during the strong phase, particularly north of 20° N. The difference in the air temperature is larger in boreal winter (Fig. 2b), with values higher than 10° in the sub-polar gyre and the GIN seas, which may be linked to the intensified deep convection. The Arctic and Scandinavia warm 2°–3° and Europe 1°–2° during the strong AMOC phase with respect to the weak one. A similar pattern occurs during boreal summer (Fig. 2c), although intensities are smaller, reaching a maximum difference of 5° in the Labrador and GIN seas. The changes in precipitation comprise an increase in the sub-polar gyre and the GIN seas during DJF (Fig. 2d) and a northward shift of the ITCZ. The latter is displayed as an increase in precipitation north of the equator and a decrease in precipitation south of the equator in JJA. The magnitude of the changes reaches values up to 1.5 mm day^{-1}, which is more than two times the magnitude of the high-frequency variability. Indeed, the standard deviation of the JJA precipitation averaged in the Atlantic box around the ITCZ (60° W–0; 10° S–10° N) is 1 mm day^{-1} for the low-frequency variability and 0.4 mm day^{-1} for the high-frequency variability (cutoff period of 30 years). The meridional shift of the ITCZ, which is associated with an anomalous

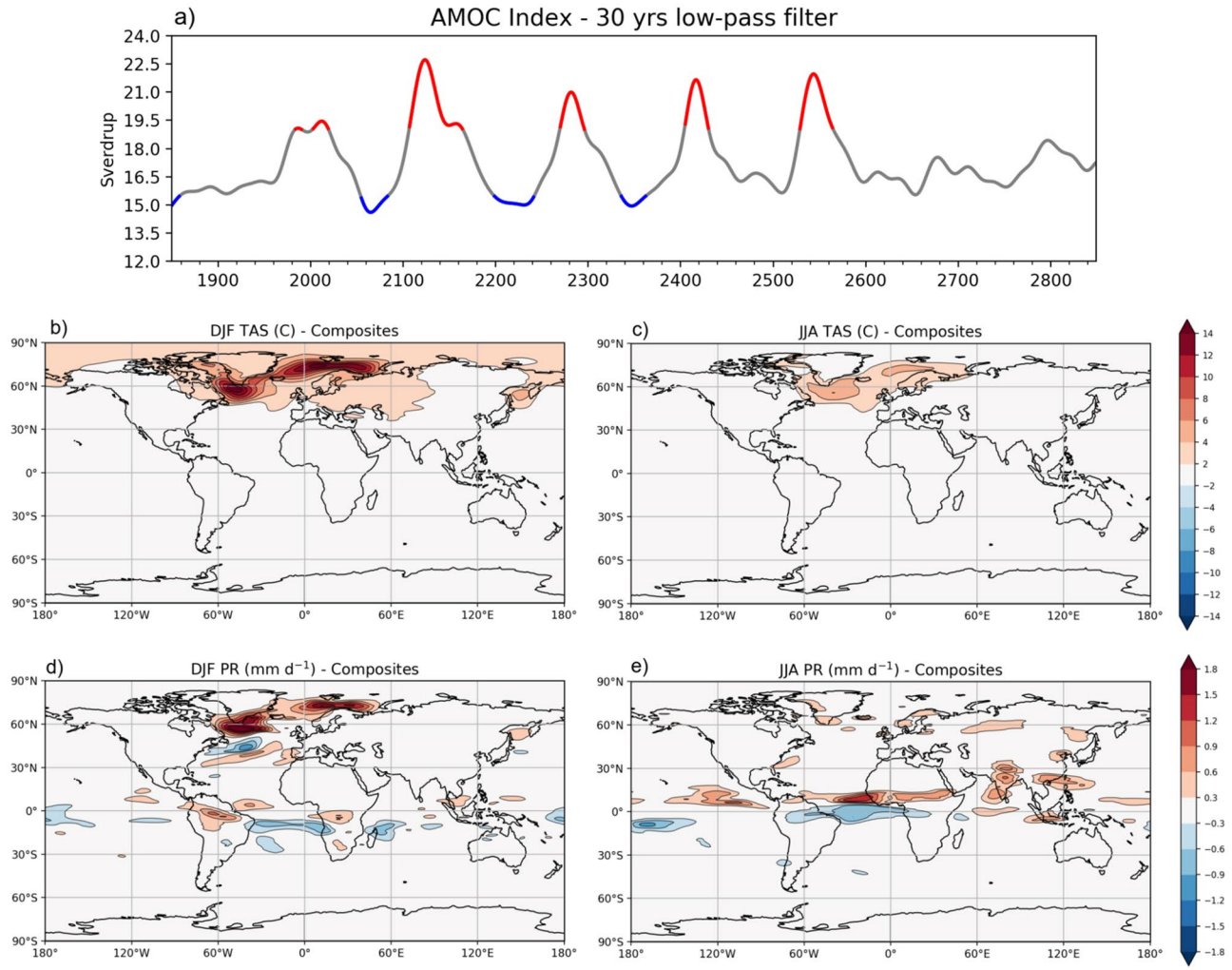

Fig. 2 **a** Time-series of the 30-year low-pass filtered AMOC index. The strong and weak AMOC events are highlighted in red and blue, respectively. The 2-m air temperature (C) difference between the composites for strong and weak AMOC events for **b** DJF and **c** JJA. The difference in precipitation (mm day^{-1}) between the composites for strong and weak AMOC events for **d** DJF and **e** JJA

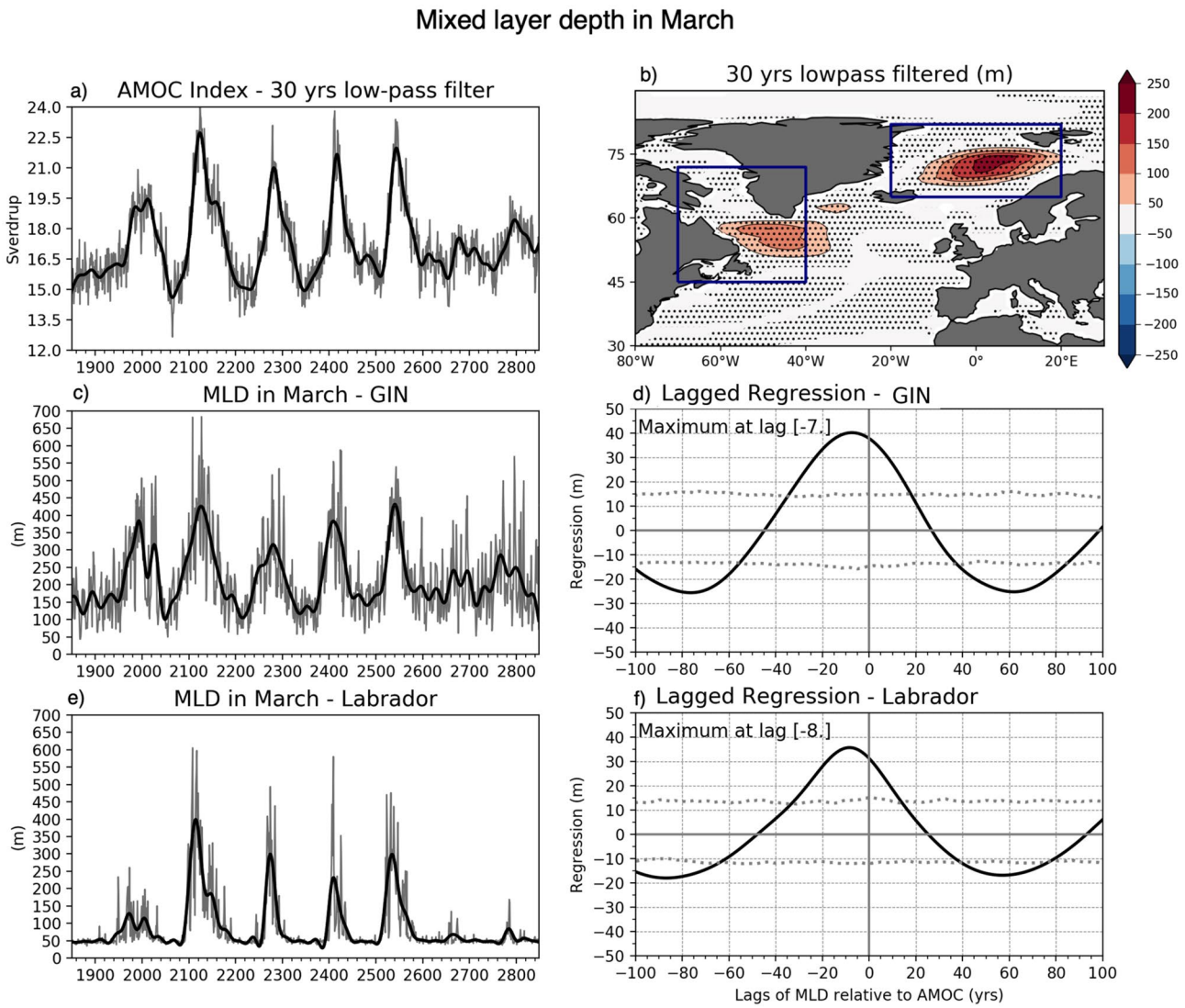

Fig. 3 **a** Time-series of AMOC index. **b** Low-frequency MLD (m) in March in the North Atlantic regressed on the AMOC index. **c**, **e** Time-series of the mean MLD in March in the GIN and Labrador seas, respectively. **d**, **f** Lagged regressions between the AMOC index and the MLD in March in the GIN and Labrador seas. Positive lags indicate that AMOC leads MLD, and negative lags indicate that MLD leads AMOC. Blue boxes in **b** indicate the Labrador and GIN regions. Dots in **b** and dotted lines in **d** and **f** show the significance at a 95% confidence level

Hadley circulation, is a known feature of the climate response to changes of the AMOC (e.g. Zhang and Delworth 2005) or also the response to imposed changes of ice cover in the Northern Hemisphere (Chiang and Bitz 2005). Motivated by these large impacts on the atmosphere, we now focus on understanding the mechanisms of AMOC oscillations.

3.1 Mechanism behind the multi-centennial AMOC oscillations

North Atlantic deep convection in EC-Earth3 is concentrated in the Labrador Sea and the GIN seas. However, the low-frequency variability of the mixed layer depth (MLD) in March, in association with changes in the AMOC, is more intense in the GIN seas than in the Labrador Sea (Fig. 3b). The time-series of MLD in March for the two areas (Fig. 3c, e) covary with the AMOC index (Fig. 3a). Indeed, the correlation (lag 0) between the low-frequency variability (period >30 years) of the AMOC and the MLD is 0.84 and 0.77 for the GIN seas and the Labrador Sea, respectively. The lagged regression analysis (Fig. 3d, f) reveals that the MLD variations in the GIN and Labrador lead the AMOC index variations by 7 and 8 years, respectively. This suggests that the low-frequency AMOC variability is modulated by the low-frequency variability of the stratification in those areas. Indeed, the upper 300 m mean potential density leading the

AMOC index by 7 years is characterized by significant positive anomalies in the GIN and Labrador seas and negative anomalies in the central Arctic (Fig. 4a). This means that around 7 years before a maximum AMOC, the sites of deep convection display positive anomalies of upper-layer density, facilitating the deep water formation.

Seawater potential density depends on temperature and salinity. We investigated the contributions to changes in potential density (black lines in Fig. 4c–h) from temperature (red lines) and salinity (blue lines) for the Arctic, GIN seas and the Labrador Sea. The time-series are plotted in Fig. 4c, e and g, respectively. The lagged regressions between those time-series and the AMOC index are plotted in Fig. 4d, f and h. It is clear that changes in the upper-layer salinity dominate the low-frequency variability of the potential density in these areas. In the Arctic and the Labrador Sea, the thermal contribution to the density anomalies is negligible. In the GIN seas, it has a small contribution but acts in the opposite direction. Indeed, north of ~ 50°N, the pattern of upper-layer salinity regressed on the AMOC index (Fig. 4b) resembles the density one (Fig. 4a), with a negative anomaly in the central Arctic and positive anomalies in the areas of deep convection and the northern coast of Greenland, North America and Siberia. The pattern of the mean salinity between 300 and 1500 m regressed on the AMOC index (not shown) also shows positive anomalies in the GIN and Labrador seas and negative anomalies in the central Arctic, but with smaller absolute values. Moreover, the lagged regressions (Fig. 4d, f and h) show that the maximum of AMOC occurs between 5 and 10 years after the maximum of upper-layer salinity in the GIN and Labrador seas (in agreement with the MLD) and between 40 and 50 years after the maximum in the central Arctic. Thus, we conclude that the salinity field is a robust indicator for density anomalies.

So far, we have shown that the multi-centennial AMOC fluctuations are preceded by changes in the upper-layer salinity in the GIN and Labrador seas. At the same time, the Arctic displays salinity anomalies of the opposite sign. The Hovmöller diagram of salinity for the North Atlantic (Fig. 5a) reveals that salinity anomalies are highest in the Arctic and clearly propagate southward from 90° N to 75° N. It is possible to notice that the salinity anomalies in the Arctic experience fast transitions from positive to negative values in synchrony with the southward propagation. Figure 5a thus suggests that low-frequency AMOC variability is modulated by salinity anomalies accumulated in the Arctic that propagate into the North Atlantic, thereby affecting the water column stability in the areas of deep water formation. Hence,

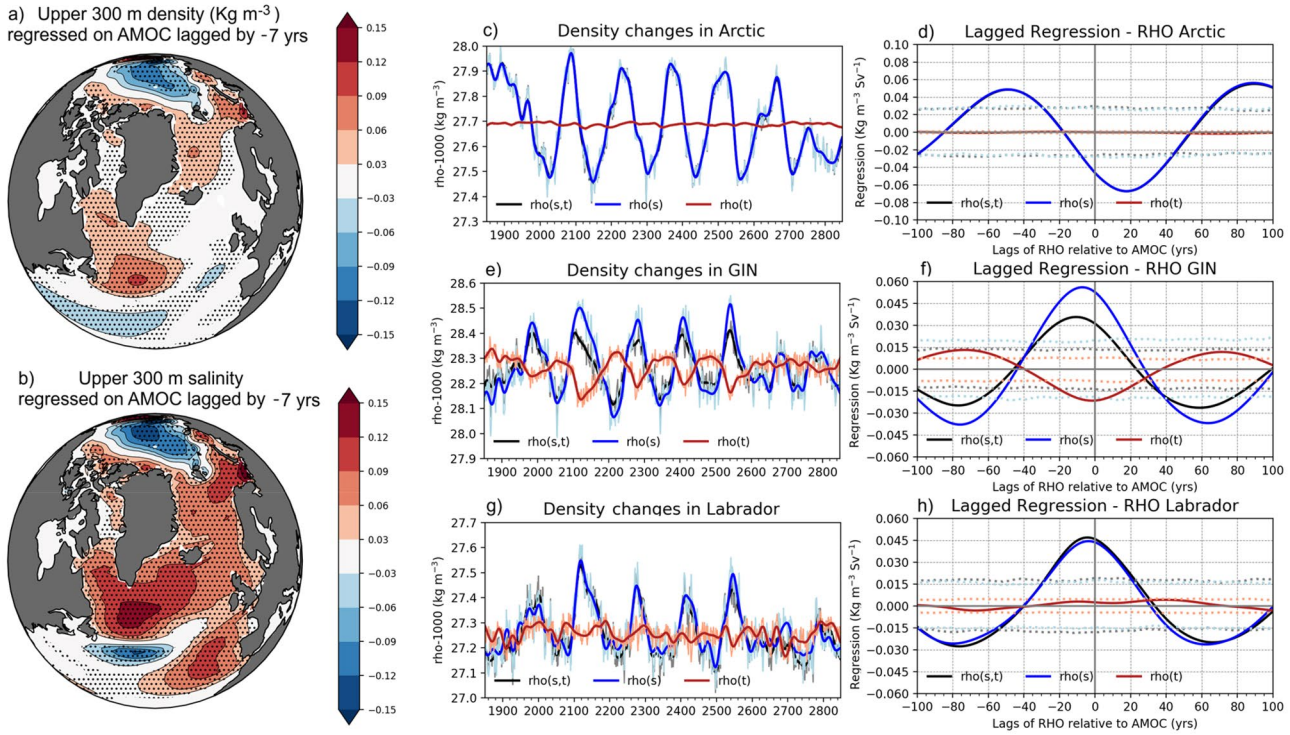

Fig. 4 **a**, **b** 300 m upper-layer potential density (kg m^{-3}) and salinity (psu), respectively, regressed on the AMOC index lagged by − 7 years. **c**, **e**, **g** Time-series of the potential density and the salinity and temperature contributions to changes in the potential density for the Arctic, GIN seas and the Labrador Sea, respectively. **d**, **f**, **h** Lagged regressions of the density and the salinity and temperature contributions to changes in density on the AMOC index. Positive lags indicate that AMOC leads RHO, and negative lags indicate that RHO leads AMOC. Dots in **a** and **b** and dotted lines in **d**, **f** and **h** show significance at a 95% confidence level

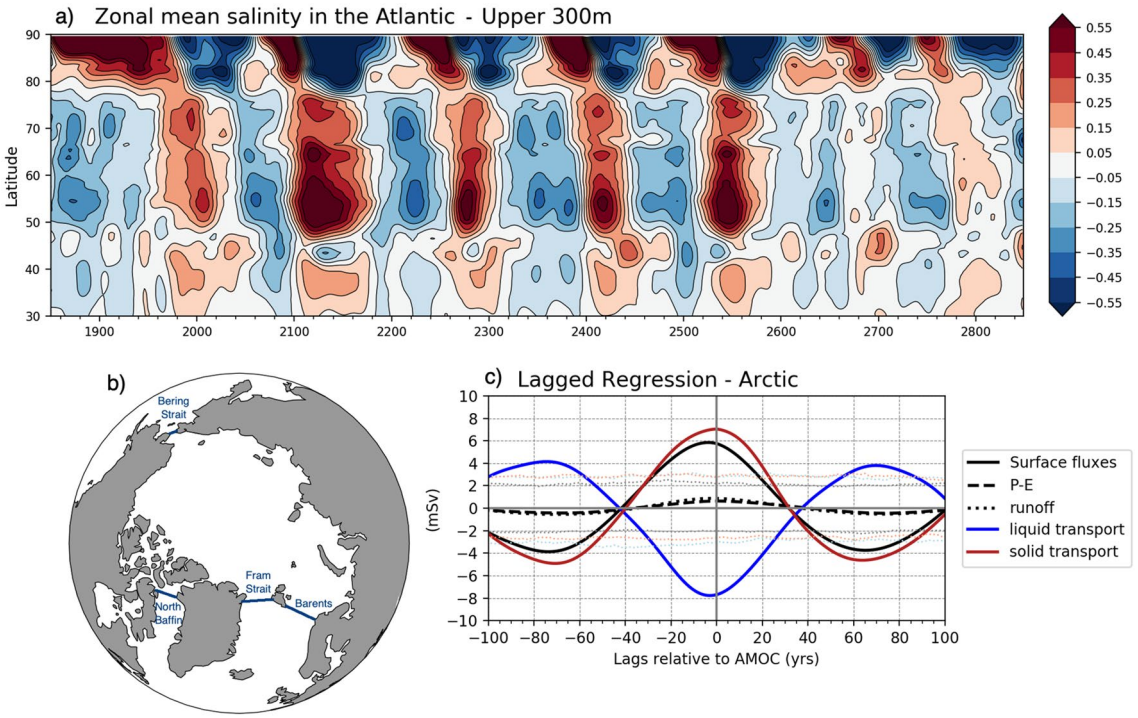

Fig. 5 **a** Salinity anomalies (psu) in the upper 300 m of the Atlantic Ocean as a function of time and latitude. **b** Position of the straits that connect the Arctic to the open ocean. **c** Components of the freshwater fluxes in the Arctic regressed on the AMOC index. Positive lags indicate that AMOC leads freshwater flux or transport, and negative lags indicate that freshwater flux or transport leads AMOC. Dots indicate significance at a 95% confidence level in **c**

in what follows, we investigate the freshwater budget in the Arctic Ocean, which may explain the AMOC variability.

Freshwater in the Arctic can be modified by surface freshwater fluxes and freshwater transport through its boundaries or straits (Fig. 5b). The surface freshwater flux includes net precipitation (i.e., precipitation minus evaporation), river runoff and sea-ice formation and melting. The lateral transport of freshwater can be liquid (due to ocean currents carrying ocean water) or solid (due to sea-ice motion). Note that the solid freshwater does not contribute directly to changes in salinity, but it does indirectly through the availability of sea ice to be melted. The lagged regressions of the surface fluxes (black), and liquid (blue) and solid (red) freshwater transports on the AMOC index are plotted in Fig. 5c. Positive freshwater surface flux or lateral transport values indicate freshwater input to the Arctic, whereas negative values indicate freshwater export from the Arctic. Freshwater input in the Arctic by surface fluxes (black line in Fig. 5c) is maximum at lag 0 approximately, in phase with the maximum of AMOC. Net precipitation (black dashed line in Fig. 5c) and river runoff (black dotted line in Fig. 5c) marginally contribute to the surface flux variability, which is mainly accounted for by sea-ice formation and melting. This suggests that a strong AMOC is associated with sea-ice melting and consequent reduction of upper layers salinity in the Arctic. Indeed, the composites of sea-ice thickness anomalies for strong (Fig. 6a) and weak (Fig. 6b) AMOC events, as indicated in Fig. 2a, show a reduction and increase of sea ice in the Arctic, respectively. Likewise, the solid freshwater transport is maximum at lag 0, and its amplitude suggests that part of the sea ice that melts in association with a maximum AMOC comes from the open ocean and enters the Arctic through the Arctic boundaries. On the other hand, and in phase with the maximum AMOC, freshwater is exported from the Arctic due to liquid transport through the Arctic boundaries (blue lines in Fig. 5c). In summary, in association with a strong AMOC and, therefore, a strong meridional heat transport into the North Atlantic high latitudes, the Arctic accumulates freshwater mainly due to sea-ice melting and releases freshwater due to liquid transport through the straits. Also, the positive values of the regressed surface flux and solid transport are higher in absolute value than the negative ones, whereas the opposite occurs for the liquid transports. This indicates that sea ice contributes more to the import of freshwater to the Arctic than to its export. In contrast, liquid transport seems to play a dominant role in exporting freshwater from the Arctic (Fig. 5c).

To better understand the role of the exchanges between the Arctic and the open ocean, Fig. 7 shows the freshwater transports through the single straits. The 1000-year

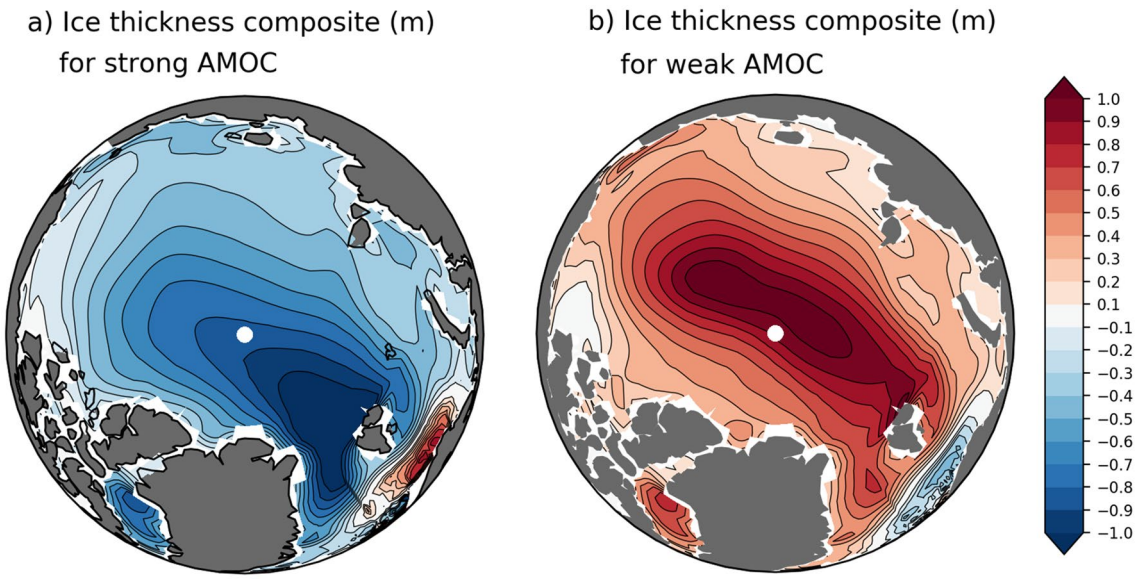

Fig. 6 Composites of sea-ice thickness (m) anomalies for **a** strong and **b** weak AMOC events as indicated in Fig. 2a

time-series of liquid (blue) and solid (red) transports are displayed in the left column, and the lagged regressions on the AMOC index are shown in the right column of Fig. 7. The liquid transport anomalies are decomposed in anomalies caused by the mean currents transporting salinity anomalies (*Sprime*, dashed blue lines) and the anomalies caused by the mean salinity transported by the current anomalies (*Vprime*, dotted blue lines). The mean terms refer to the whole 1000-year period. The anomalies caused by the salinity anomalies transported by the current anomalies (*Sprime*Vprime*) were also computed, but because the lagged regressions of this term are not significant at any lag and any strait, they are not plotted in Fig. 7. Solid freshwater transports occur through the Fram Strait and the Barents. The two are nearly in phase and import solid freshwater to the Arctic simultaneously with a maximum AMOC. Conversely, the solid freshwater transport through North Baffin and Bering Strait is almost negligible. On the other hand, the liquid transports through all the straits show a significant covariance with the AMOC. The contributions through Barents (mainly explained by *Sprime*) and Bering (entirely explained by *Vprime*) are relatively small and in phase, both maximum at lag 0. Whereas a relatively small amount of liquid freshwater is entering the Arctic through the Bering Strait (~2.5 mSv per unit of AMOC change; Fig. 7h), freshwater is being exported through Barents (~4 mSv per unit of AMOC change; Fig. 7d). However, the largest contributions of liquid freshwater exchanges between the Arctic and the open ocean occur through North Baffin and Fram Strait, and they are not in phase with the AMOC changes. The maximum freshwater export by liquid transport through North Baffin occurs between 10 and 20 years before a maximum AMOC. It is entirely explained by the term *Vprime*, that is, by the circulation anomaly that transports mean salinity (Fig. 7f). In contrast, the maximum export through the Fram Strait occurs around 30 years after a maximum AMOC in which also the *Vprime* component dominates. There is a contribution by *Sprime* too, but it is not significant (Fig. 7b, blue lines). From this, it is possible to deduce that a large amount of freshwater accumulated during a strong phase of the AMOC due to sea-ice melting, leaves the Arctic and enters the Labrador and GIN seas as liquid transport through North Baffin and Fram Strait, mainly due to current anomalies (with a minor contribution of Barents too). Although the liquid transports through North Baffin and Fram Strait appear to be not in phase with the AMOC index, summing up all the contributions, the maximum net liquid export occurs in phase with a maximum AMOC (Fig. 5b).

It seems thus plausible that the liquid freshwater, initially exiting the Arctic from North Baffin and in a second instance from the Fram Strait, is responsible for the freshening of the Labrador and GIN seas and thus operates to slow down the AMOC during its strong positive phase. This can be better appreciated by looking at Fig. 8b–e, which show the composites of the upper-layer salinity and current anomalies for different lags with respect to a strong AMOC as indicated in Fig. 2. The average fields of upper-layer salinity and current anomalies are plotted in Fig. 8a.

Let's start looking at the composites at lag 0, that is, simultaneously with a strong AMOC (Fig. 8b). As pointed out before, the maximum AMOC is associated with a positive surface temperature anomaly and consequently with a maximum freshwater input in the Arctic Ocean due to sea-ice melting. As a consequence, the interior of the Arctic

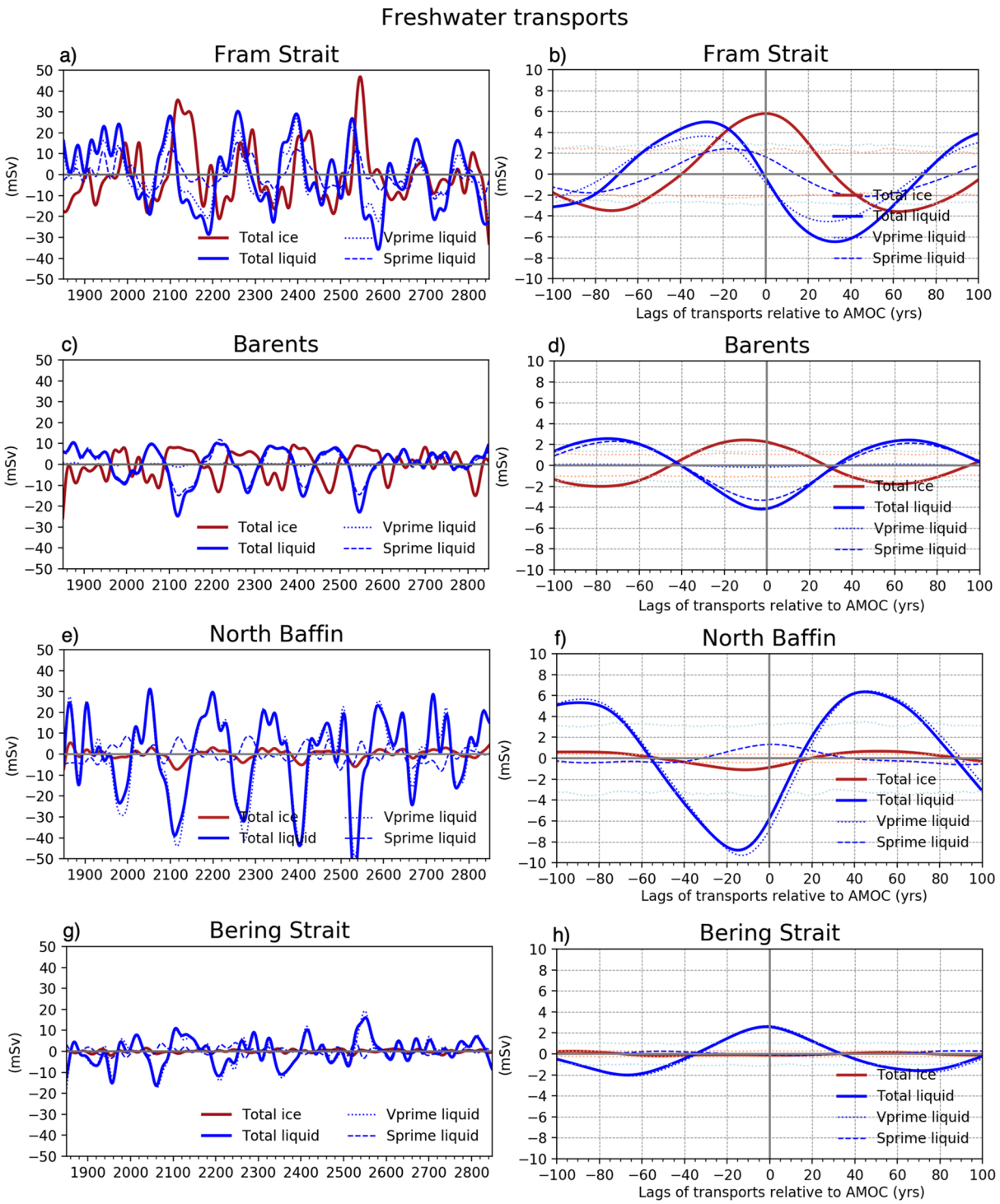

Fig. 7 Liquid (blue) and solid (red) freshwater transport into the Arctic through the boundaries indicated in Fig. 5b: the Fram Strait (**a**, **b**), Barents (**c**, **d**), the North Baffin (**e**, **f**) and the Bering Strait (**g**, **h**). The time-series of the transport anomalies are plotted in the left column, whereas the lagged regressions on the AMOC index are in the right column. The liquid freshwater transports are decomposed into the transports of the mean salinity by the current anomalies (*Vprime*, dotted blue lines) and the transports of the salinity anomalies by the mean current (*Sprime*, dashed blue lines). Positive lags indicate that AMOC leads freshwater transport, and negative lags indicate that freshwater transport leads AMOC. Dots indicate significance at a 95% confidence level in the right column plots

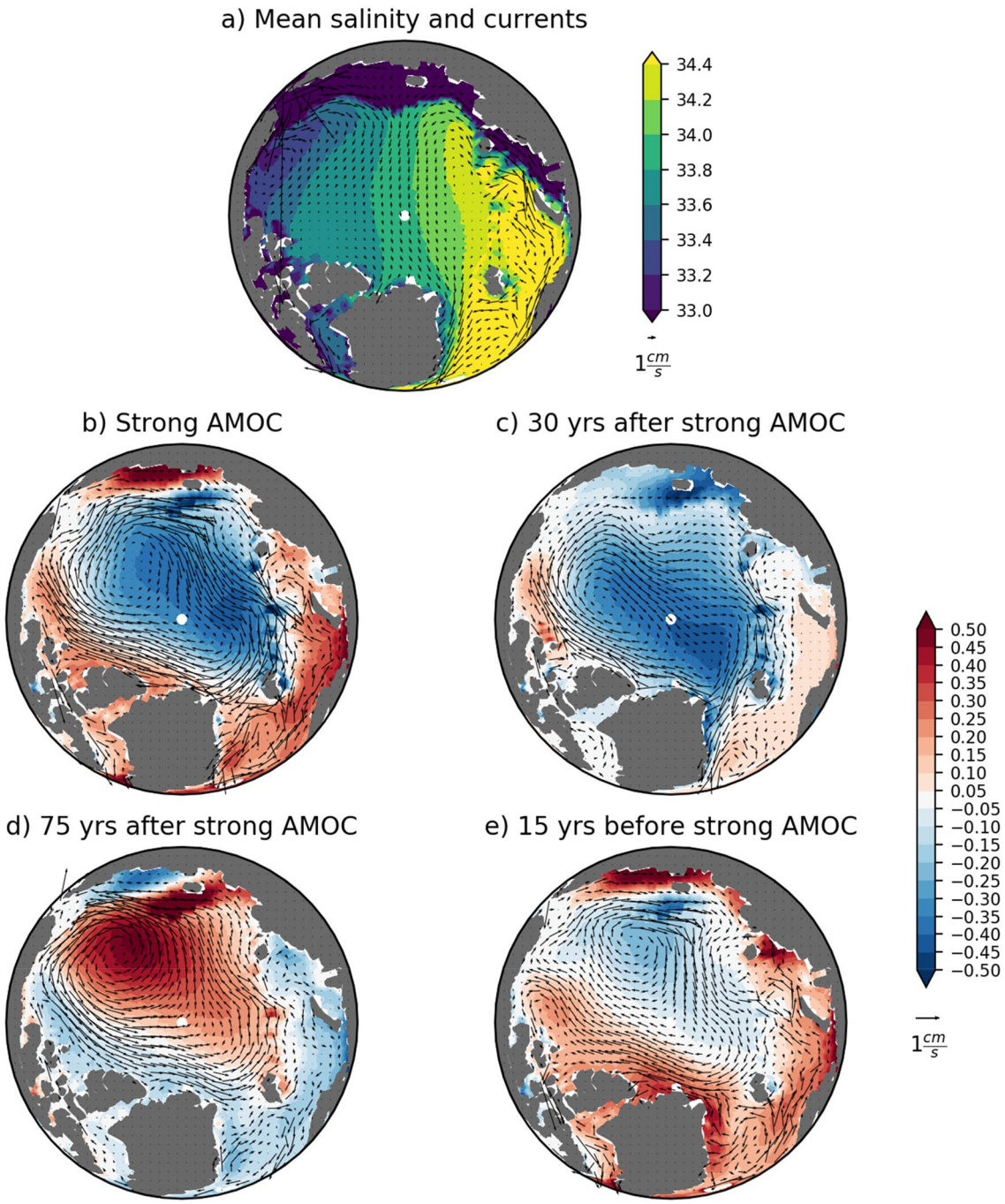

Fig. 8 **a** Mean salinity (psu) and current fields. Composites of salinity and current anomalies for **b** strong AMOC events; **c** 30 years after strong AMOC events; **d** 75 years after strong AMOC events; and **e** 15 years before strong AMOC events

Ocean exhibits a negative salinity anomaly. We do not find significant regressions between the atmospheric fields (sea level pressure and winds) in the Arctic and the AMOC index, suggesting that the oceanic circulation is not forced by the atmosphere. Indeed, the anticyclonic circulation anomaly (Fig. 8b) is consistent with the vertically integrated thermal wind relation. The anticyclonic circulation anomaly helps to keep the salinity anomaly trapped in the central Arctic and well-detached from the Fram Strait so that the latter marginally contributes to the liquid freshwater exchanges with the Arctic at lag 0 (see Fig. 8b). However, the largest freshwater export is occurring through North Baffin (Fig. 7f), and it is due to the circulation anomaly through the western Canadian archipelagos. Since the mean salinity in the Arctic is lower

than in the North Atlantic, the term *Vprime* contributes to the export of freshwater from the Arctic.

Thirty years after the peak of the AMOC (Fig. 8c), the negative salinity anomaly and the anticyclonic circulation anomaly are shifted towards the North Atlantic. This can be due to the mean currents in the Arctic that present a mean flow from Siberia to the North Atlantic (Fig. 8a). At this point, the freshwater export through Fram Strait is maximum mainly due to the circulation anomaly transporting mean salinity, *Vprime* (Fig. 7b). Indeed, the circulation anomaly presents a strong southward component at the Fram Strait (Fig. 8c). As in the case of North Baffin, since the mean salinity in the Arctic is lower than in the North Atlantic, the term *Vprime* contributes to the export of freshwater from the Arctic. As a result, as the GIN seas become fresher, the water column stabilizes, inhibiting deep water formation. This way, the AMOC further slows down, less heat is transported to the high latitudes of the Northern Hemisphere and sea ice forms, contributing to an accumulation of relatively salty waters in the Arctic.

Around 75 years after a strong AMOC (Fig. 8d), roughly half of the complete period and, therefore, a minimum of AMOC is expected, the formation of sea ice contributes to an increase in salinity in the central Arctic. As a consequence, in thermal wind balance, the circulation reverts to a cyclonic one, which prevents currents from crossing the Fram Strait, minimising the freshwater's liquid transport there (Figs. 7b and 8d). Some freshwater is entering the Arctic through Barents (Fig. 7d) due to the term *Sprime*, that is, salinity anomalies (fresher in the GIN seas with respect to the Arctic) transported by the mean currents that have a northward component there (Fig. 8a). Also the North Baffin presents at lag 75 import of freshwater anomalies into the Arctic due to the term *Vprime* (Fig. 7b).

By lag − 15 years (that is 15 years before a maximum AMOC; Fig. 8e), the AMOC has already increased, so the poleward heat transport that produces a melting of the sea ice and thus contributes to the formation of the freshwater anomaly in the Arctic. Again, the cyclonic circulation associated with the previous minimum AMOC is shifted towards the North Atlantic, probably transported by the mean currents that have that direction (Fig. 8a). The resulting local circulation close to North Baffin has a strong southeast component, favouring the liquid freshwater transport through North Baffin that results maximum (Fig. 7f) due to the term *Vprime*. This leads to a new reduction of the AMOC intensity in a new cycle.

In summary, the mechanism can be explained by the accumulation of upper-layer salinity anomalies in the Arctic and its circulation-induced release to the North Atlantic, which modify the vertical density profiles in the deep convection regions that directly affect the meridional overturning circulation. The sea-ice formation and melting controlled by the poleward ocean heat transport due to the AMOC are the main contributors to the accumulation of freshwater anomalies in the Arctic, providing negative feedback to control the increase and reduction of the AMOC. The mechanism is mediated by the liquid freshwater transports through the Arctic boundaries, which are the main responsible for the exchange of freshwater anomalies with the open ocean. Whereas the net liquid freshwater transport is in phase with the AMOC changes, the single contributions through North Baffin and Fram Strait are not, suggesting a complementary mechanism by the two regions. In particular, the maximum freshwater export from the Arctic through North Baffin results from local circulation anomaly which is associated with the large scale cyclonic anomaly generated during the previous minimum of AMOC that was already transported towards the North Atlantic by the mean currents. Conversely, the maximum export of freshwater through Fram Strait is dominated by local circulation anomaly which is associated with the anticyclonic circulation anomaly generated during the previous maximum of AMOC that is shifted towards the North Atlantic.

3.2 What happens in a warmer climate?

The 500-year time-series and power spectral density of the AMOC index for five different runs are plotted in Fig. 9. They include part of the *piControl* analysed above (black) and four other quasi-equilibrium simulations forced with fixed conditions corresponding to the years 1990 (*b990*, brown), 2025 (*b025*, blue), 2050 (*b050*, green) and 2100 (*b100*, red) described in Sect. 2.1. The runs start from the climate conditions of the years 1990, 2025, 2050 and 2100, reached through the historical + SSP5.85 scenario. The final mean temperature increase for the four simulations is about 1.3°, 2.7°, 4.5° and 9.4°, respectively, with respect to pre-industrial conditions (Fabiano et al., in preparation). Time-series are detrended before computing the spectra. The power spectral density of the AMOC index for the *piControl* run (Fig. 9b) considers the first 500 years to facilitate the comparison to the other simulations, which are 500-year long. Note that the *y*-axis in Fig. 9b, c differ. On the one hand, the mean AMOC index value decreases with warming under the SSP5.85 future scenario, being 17.21 Sv in the *piControl* run and 15.16 in *b050*. In *b990*, however, the mean value is 17.81, slightly higher than in the pre-industrial run. On the other hand, the multi-centennial variability in the pre-industrial climate seems to damp in a warmer climate (Fig. 9a). Indeed, the standard deviation of the low-frequency variability (periods higher than 30 years) is 1.96 Sv in the *piControl* run, and it is less than 0.9 Sv in all the other experiments. Besides, the power spectra density of the *piControl* is, by far, dominated by a ~150 years variability (Fig. 9b). In the *b990, b050* and *b100* experiments, there is

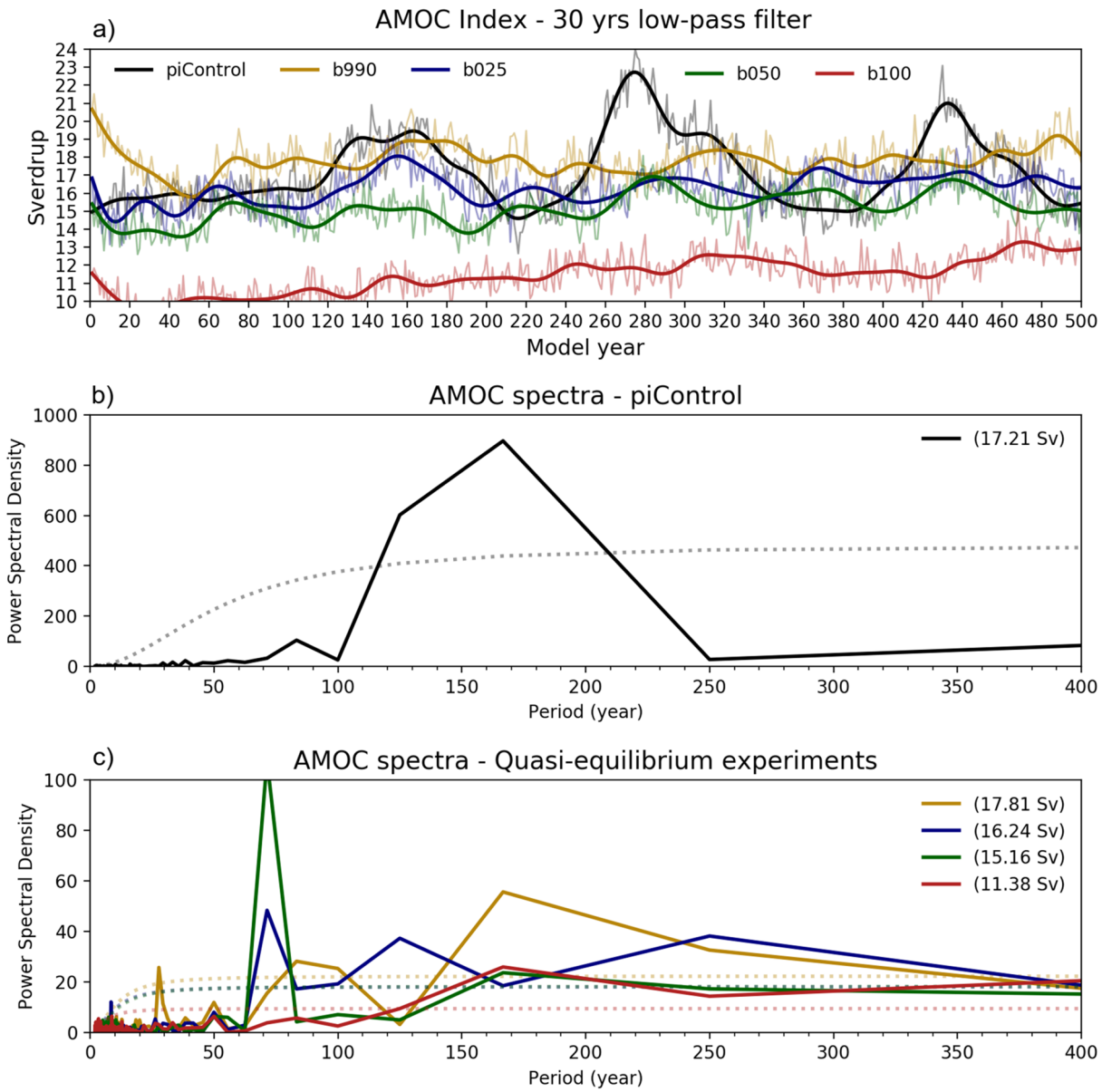

Fig. 9 **a** Annual (thin lines) and 30 year low-pass filtered (thick lines) AMOC index for the first 500 years of *piControl* (black), *b990* (brown), *b025* (blue), *b050* (green) and *b100* (red), representing different quasi-equilibrium climates. **b** power spectral density of the AMOC index for the first 500 years of *piControl*. **c** Power spectral density of the AMOC index for *b990* (brown), *b025* (blue), *b050* (green) and *b100* (red). Significance at 95% confidence level in **b** and **c** are indicated by dots. The mean values of the AMOC index for each run are displayed between brackets in **b** and **c**

still a signal at ~ 160 years (Fig. 9c), but the power spectra density is almost two orders of magnitude lower than in the *piControl* run. In the *b025* and *b050* experiments, the multi-decadal variability dominates.

In summary, looking at the *b990*, *b025*, *b050* and *b100* experiments, it seems that the multi-centennial AMOC variability that dominates the power spectra density in the pre-industrial climate attenuates with warming. We hypothesize that this mode of variability is state-dependent. We showed in Sect. 3.2 that the melting or formation of the sea ice associated with a strong or weak AMOC plays an important role in developing a salinity anomaly in the Arctic that is released to the open ocean by the liquid exchanges through the Arctic boundaries. We speculate that in a warmer climate with respect to the pre-industrial one, the availability of sea ice to be melted is reduced and so is the self-sustained mode.

For example, Fig. 10 shows the mean sea-ice thickness (Fig. 10a, b), salinity and currents (Fig. 10c, d) for the *piControl* and *b050*. The mean sea-ice thickness in the central Arctic presents values between 3.5 and 5.5 m in the

piControl (Fig. 10a) and below 1 m in *b050* (Fig. 10b). This suggests that in a warmer climate, there is no sea ice available to melt which can contribute to the surface freshwater flux that produces the large negative salinity anomaly during a strong AMOC phase in the *piControl* run. In fact, the regression between the freshwater surface flux on the AMOC index is not significant at any lag in the *b050* experiment (not shown). On the other hand, the mean upper-layer salinity in the central Arctic displays much larger spatial gradients and associated currents in *b050* (Fig. 10d) than in *piControl* (Fig. 10c). This, together with the low amount of sea ice cover, favours a fast exchange of liquid freshwater between the Arctic and the GIN seas. In fact, on average, liquid freshwater leaves the Arctic Ocean through North Baffin, Fram Strait, and Barents and enters the Arctic Ocean through the Bering Strait (Table 1). The liquid transport's absolute values, in general, increase with warming, as one may expect since the region is less covered by sea ice in the warm climate. In contrast, the mean solid freshwater transports decrease in absolute value with warming, even reaching null values (Table 1). Overall, we conclude that the intensity and even existence of the multi-centennial AMOC variability would depend on the mean climate.

4 Final remarks

We report the presence of low-frequency variability in the AMOC simulated by EC-Earth3 under pre-industrial conditions. These oscillations have a period of around 150 years. We find that the build-up of salinity anomalies in the Arctic and their release into the North Atlantic affect the area of deep-water formation and modulate AMOC variability on centennial timescales. The proposed mechanism is summarized in Fig. 11, in which the blue arrows represent the path from a strong AMOC to a weak one, and the red arrows represent the recovery toward a strong AMOC again. Specifically, a strong AMOC effectively transports heat into the

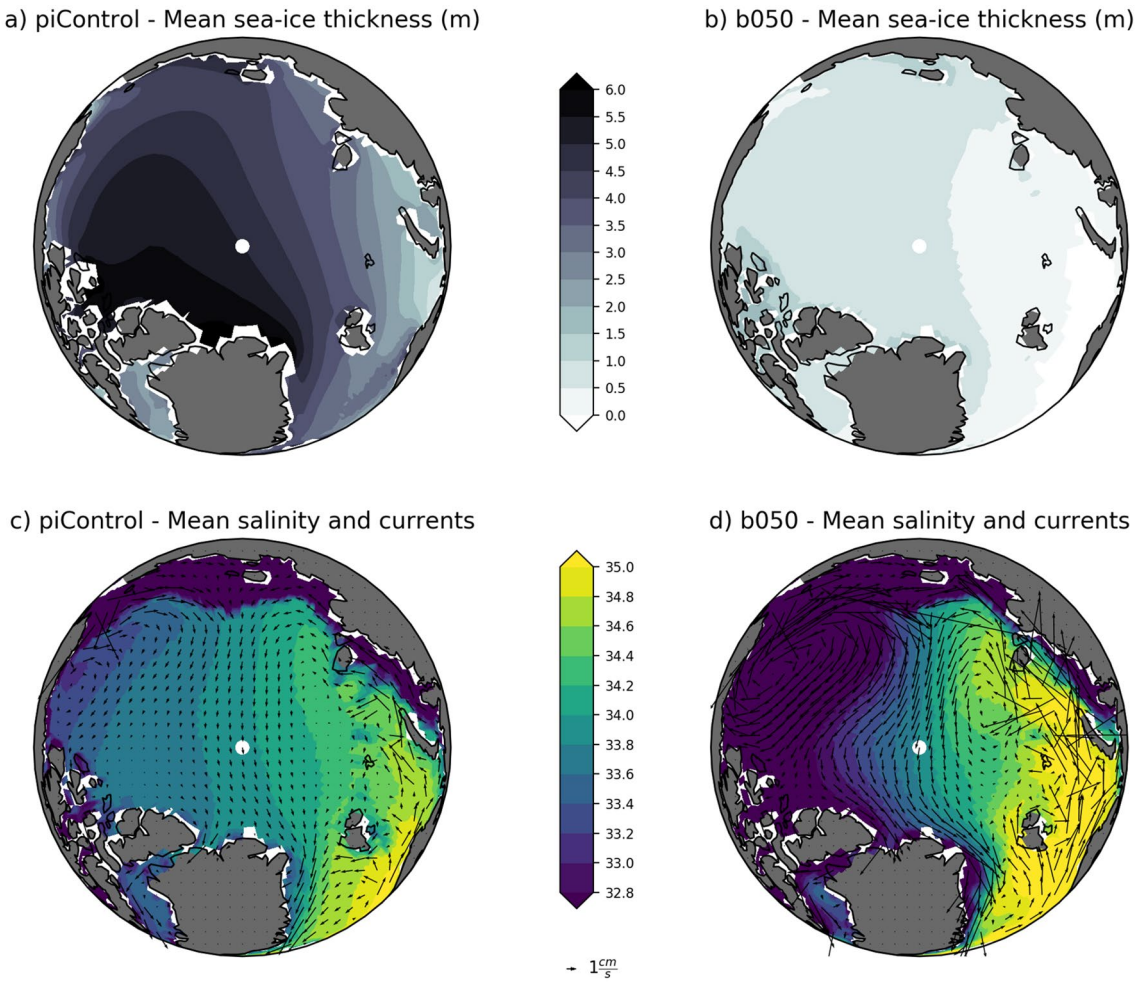

Fig. 10 **a**, **b** Mean sea-ice thickness (m) for the *piControl* and *b050*, respectively. **c**, **d** Mean upper-layer salinity (psu) and currents for the *piControl* and *b050*, respectively

Table 1 Mean liquid and solid freshwater transports through the Fram Strait, the Barents, the North Baffin and the Bering Strait for the *piControl*, *b990*, *b025*, *b050* and *b100* runs

	Mean liquid freshwater transport into the Arctic (mSv)				Mean solid freshwater transport into the Arctic (mSv)			
	Fram Strait	Barents	North Baffin	Bering Strait	Fram Strait	Barents	North Baffin	Bering Strait
PiControl	− 34.0	− 3.5	− 75.0	118.2	− 132.2	− 12.7	− 12.0	5.0
b990	− 85.4	− 21.4	− 87.0	131.5	− 83.9	− 1.2	− 13.2	2.0
b025	− 118.7	− 36.2	− 114.8	135.8	− 27.4	− 0.2	− 10.7	0.18
b050	− 118.3	− 47.4	− 150.0	151.7	− 7.5	0.0	− 7.2	− 0.3
b100	− 106.14	− 39.2	− 277.4	155.2	− 0.3	0.0	− 0.5	− 1.1

high latitudes of the North Atlantic, favouring the sea-ice melting in the North Atlantic and Arctic, particularly around Greenland and north of Svalbard. The upper-layer salinity and consequently the density in the Arctic reduce. A reduced density yields a high sea surface height and an anticyclonic circulation, trapping the salinity anomaly inside the Arctic. As a combination of the resulting circulation anomaly and the mean currents, freshwater exits the Arctic and enters the North Atlantic as liquid transport through North Baffin, Fram Strait and Barents. The maximum export of freshwater through Barents is in phase with a maximum AMOC, but the maximum exports through North Baffin and Fram Strait are not. A local cyclonic circulation anomaly occurring around 15 years before a strong AMOC helps to enhance the freshwater export through North Baffin. This local circulation is related to the large scale cyclonic anomaly generated during the previous minimum AMOC phase and transported by the mean currents towards the North Atlantic. Instead, the maximum through Fram Strait occurs around 30 years after the maximum AMOC. It is induced by a local anticyclonic circulation anomaly generated during the strong AMOC in the central Arctic and transported towards the North Atlantic by the mean currents. As a result, the net liquid freshwater export from the Arctic is in phase with a maximum AMOC. This input of freshwater into the Labrador and GIN seas stabilises the water column that inhibits the deep-water formation, and as a consequence, the AMOC reduces. A weak AMOC transports less heat to the North Atlantic, constraining the sea-ice melting and producing a positive salinity anomaly in the Arctic. This reverts the circulation; the freshwater export from the Arctic into the North Atlantic is minimum, favouring a positive salinity anomaly in the areas of deep convection, which helps to increase the AMOC again.

On the one hand, sea ice plays a crucial role in creating the salinity anomalies in the Arctic in phase with the AMOC

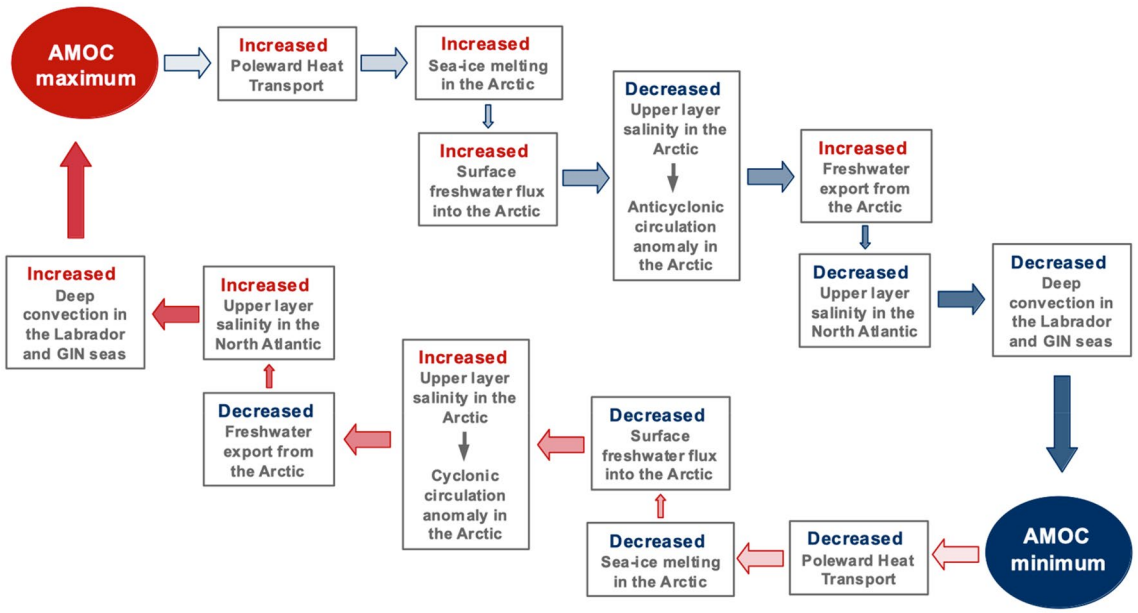

Fig. 11 Scheme summarizing the mechanisms of the multi-centennial AMOC variability simulated by EC-Earth3 under pre-industrial conditions. Blue arrows represent the path from a strong AMOC to a weak one, and red arrows represent the recovery toward a strong AMOC again

cycle. The solid freshwater import into the Arctic through the Fram Strait modifies the sea-ice thickness distribution contributing to the availability of sea ice to be melted in the Arctic during a strong AMOC. On the other hand, the liquid freshwater export from the Arctic through its boundaries is essential to propagate the salinity anomaly into the North Atlantic.

We here hypothesize that the above-described mode of variability depends on the mean state of the climate. In our *piControl* run with a mean AMOC index of ~ 17.5 Sv, these oscillations have a period of around 150 years and an amplitude of 6 Sv approximately (from crest to trough). However, in a warmer climate, the water column in the deep-water formation regions of the North Atlantic tends to stabilize. Consequently, the AMOC is expected to reduce (e.g. Bellomo et al. 2021). Further, sea-ice cover and thickness in the GIN seas and around Greenland and Svalbard are very sensitive to warming. Sea ice tends to disappear in a future scenario with a mean surface air temperature about 4.5° warmer than in the pre-industrial period. Moreover, the mean upper-layer salinity in the Arctic shows larger spatial gradients and consequently stronger mean currents in a warmer climate. Therefore, we believe that the conditions mentioned above for maintaining the multi-centennial fluctuations, namely the surface freshwater fluxes due to sea-ice melting and formation in the Arctic and the exchanges of the freshwater by liquid transport through the Arctic boundaries, change with warming. As a consequence the self-sustained mechanism tends to dampen.

We are aware that the simulations explored in Sect. 3.2 are partially limited by their duration since 500 years might not be enough to achieve equilibrium, and climate variability could potentially depend on the transient forcing. However, the fact that (a) no centennial to multi-centennial cycles can be observed even at the end of the simulations (Fig. 9a); (b) the difference between the power spectral density with respect to the *piControl* is of more than one order of magnitude (Fig. 9b, c); and (c) all the experiments explored in Sect. 3.2 behave consistently, we could conclude that the oscillations tend to damp with warming and the self-sustained oscillatory mechanism could be state-dependent.

The mechanism for describing the low-frequency self-sustained AMOC variability in EC-Earth3 is very similar to the one found in IPSL-CM6-LR (Jiang et al. 2021). The authors showed that the AMOC fluctuations in their model are preceded by density anomalies driven by salinity in the main deep convection sites. The salinity anomaly comes from the accumulation and release of freshwater in the Arctic. Both models, EC-Earth3 and IPSL-CM6-LR, share the same ocean model, ocean grid and sea-ice model, although the atmospheric component differs. The main difference between the two models is the amplitude and period of the oscillations. The amplitude of the oscillations is larger in EC-Earth3 (~ 6 Sv) than in IPSL-CM6-LR (< 3 Sv). This discrepancy may be associated with the mean AMOC value. The mean Atlantic meridional streamfunction at 30°N is 10.8 Sv in IPSL-CM6-LR (Jiang et al. 2021) and 16.25 Sv in EC-Earth3. Also, the period of the fluctuations slightly differs: whereas it was reported to be approximately 200 years for IPSL-CM6-LR, we found a shorter period of about 150 years in EC-Earth3. We speculate that the multi-centennial time-scale is determined by the dimension of the Arctic basin and the time needed to export the freshwater from the Arctic into the North Atlantic. However, the differences in the features of the fluctuations between the models could be associated with a different mean state, particularly the mean salinity, temperature, currents and sea-ice cover and volume in the North Atlantic and the Arctic. Indeed, even if EC-Earth3 captures well the sea-ice area in the Arctic, there are large regional biases in the sea-ice concentration. In particular, the model overestimates the sea-ice concentration in March near the ice margins in the Atlantic, that is, in the Labrador, GIN and Barents seas (Figs. 10 and 11 from Döscher et al. 2022). The characteristics of the multi-centennial oscillations reported here probably change if the model bias of sea ice in the Arctic is reduced.

To what extent these modelled oscillations can be considered model features, or a real phenomenon remains. There is evidence of events of multi-centennial fluctuations of the AMOC in paleoclimate records. For example, Mann et al. (1995) studied a set of global temperature proxy records of several centuries duration. They found evidence for centennial natural climate variability exhibiting high amplitude confined to the North Atlantic and Arctic. More specifically, Ayache et al. (2018) found multi-centennial variations in an AMOC reconstruction based on 22 proxy SST records compiled in the North Atlantic during the Holocene. On the other hand, Oppo et al. (2003) investigated changes in the carbon-isotope composition of benthic foraminifera throughout the Holocene as a proxy of the deep-water formation in the North Atlantic. They found variations on a centennial–millennial timescale. Laepple and Huybers (2013) also found centennial to millennial variability when analysing the late-Holocene marine temperature from Mg/Ca and Uk37 proxies.

Finally, the presence of such low-frequency variability modelled by EC-Earth3 and IPSL-CM6A-LR can affect the estimation of the transient climate sensitivity. Along this line, Bonnet et al. (2021) analysed 32 historical simulations performed with the IPSL-CM6A-LR model. They found that the members with a large internally-driven weakening of the AMOC have, indeed, the lowest rates of global warming over the past few decades.

Acknowledgements This is TiPES contribution #158. This project has received funding from the European Union's Horizon 2020

research and innovation programme under Grant agreement no. 820970 (TiPES). KB has received funding from the European Union's Horizon 2020 research and innovation programme under the Marie Skłodowska-Curie grant agreement No. 101026907 (CliMOC). The simulation *b050* has been carried out at ECMWF under the special project SPITMECC.

Funding This is TiPES contribution #158. This project has received funding from the European Union's Horizon 2020 research and innovation programme under Grant agreement no. 820970 (TiPES). KB has received funding from the European Union's Horizon 2020 research and innovation programme under the Marie Skłodowska-Curie grant agreement No. 101026907 (CliMOC). The simulation *b050* has been carried out at ECMWF under the special project SPITMECC.

Data availability The model output and the scripts for analysing the data and producing the figures will be available from the corresponding authors upon reasonable request.

Declarations

Conflict of interest The authors have no relevant financial or non-financial interests to disclose.

References

Aagaard K, Carmack E (1989) The role of sea ice and other freshwater in the Arctic circulation. J Geophys Res 94:14485–14498. https://doi.org/10.1029/JC094iC10p14485

Årthun M, Wills RCJ, Johnson HL, Chafik L, Langehaug HR (2021) Mechanisms of decadal North Atlantic climate variability and implications for the recent cold anomaly. J Clim. https://doi.org/10.1175/JCLI-D-20-0464.1

Ayache M, Swingedouw D, Mary Y, Eynaud F, Colin C (2018) Multi-centennial variability of the AMOC over the Holocene: a new reconstruction based on multiple proxy-derived SST records. Glob Planet Change 170:172–189. https://doi.org/10.1016/j.gloplacha.2018.08.016

Balsamo G, Beljaars A, Scipal K, Viterbo P, van den Hurk B, Hirschi M, Betts AK (2009) A revised hydrology for the ECMWF model: verification from field site to terrestrial water storage and impact in the integrated forecast system. Hydrometeorology 10:623–643. https://doi.org/10.1175/2008JHM1068.1

Bellomo K, Angeloni M, Corti S, von Hardenberg J (2021) Future climate change shaped by inter-model differences in Atlantic meridional overturning circulation response. Nat Commun 12:3659. https://doi.org/10.1038/s41467-021-24015-w

Bjerknes J (1964) Atlantic air–sea interaction. Adv Geophys 10:1–82. https://doi.org/10.1016/S0065-2687(08)60005-9

Böning CW, Scheinert M, Dengg J, Biastoch A, Funk A (2006) Decadal variability of subpolar gyre transport and its reverberation in the North Atlantic overturning. Geophys Res Lett 33:L21S01. https://doi.org/10.1029/2006GL026906

Bonnet R, Swingedouw D, Gastineau G, Boucher O, Deshayes J, Hourdin F, Mignot J, Servonnat J, Sima A (2021) Increased risk of near term global warming due to a recent AMOC weakening. Nat Commun 12:6108. https://doi.org/10.1038/s41467-021-26370-0

Broecker WS, Peteet DM, Rind D (1985) Does the ocean–atmosphere system have more than one stable mode of operation? Nature 315(6014):21–26. https://doi.org/10.1038/315021a0

Bryan K (1962) Measurements of meridional heat transport by ocean currents. J Geophys Res 67(9):3403–3414. https://doi.org/10.1029/JZ067i009p03403

Buckley MW, Marshall L (2016) Observations, inferences, and mechanisms of the Atlantic Meridional Overturning Circulation: a review. Rev Geophys 54(1):5–63. https://doi.org/10.1002/2015RG000493

Caesar L, McCarthy GD, Thornalley DJR et al (2021) Current Atlantic Meridional Overturning Circulation weakest in last millennium. Nat Geosci 14:118–120. https://doi.org/10.1038/s41561-021-00699-z

Chiang JCH, Bitz CM (2005) Influence of high latitude ice cover on the marine Intertropical Convergence Zone. Clim Dyn 25:477–496. https://doi.org/10.1007/s00382-005-0040-5

Clark PU, Pisias NG, Stocker TF, Weaver AJ (2002) The role of the thermohaline circulation in abrupt climate change. Nature 415(6874):863–869. https://doi.org/10.1038/415863a

Cunningham SA, Kanzow T, Rayner D, Baringer MO, Johns WE, Marotzke J, Longworth HR, Grant EM, Hirschi JJM, Beal LM, Meinen CS, Bryden HL (2007) Temporal variability of the Atlantic meridional overturning circulation at 26.5 degrees N. Science 317(5840):935–938. https://doi.org/10.1126/science.1141304

Danabasoglu G et al (2016) North Atlantic simulations in coordinated ocean-ice reference experiments phase II (CORE-II). Part II: inter-annual to decadal variability. Ocean Model 97:65–90. https://doi.org/10.1016/j.ocemod.2015.11.007

Delworth TL, Zeng F (2012) Multicentennial variability of the Atlantic meridional overturning circulation and its climatic influence in a 4000 year simulation of the GFDL CM2.1 climate model. Geophys Res Lett 39:L13702. https://doi.org/10.1029/2012GL052107

Deshayes J, Frankignoul C (2008) Simulated variability of the circulation in the North Atlantic from 1953 to 2003. J Clim 21(19):4919–4933. https://doi.org/10.1175/2008JCLI1882.1

Döscher R, Acosta M, Alessandri A, Anthoni P, Arneth A, Arsouze T et al (2022) The EC-Earth3 Earth system model for the Coupled Model Intercomparison Project 6. Geosci Model Dev 15:2973–3020. https://doi.org/10.5194/gmd-15-2973-2022

ECMWF (2010). European Center for Medium Range Forecast. IFS Documentation CY36R1. https://www.ecmwf.int/en/publications/ifs-documentation. Acessed 17 Oct 2022

Eyring V, Bony S, Meehl GA, Senior CA, Stevens B, Stouffer RJ, Taylor KE (2016) Overview of the Coupled Model Intercomparison Project Phase 6 (CMIP6) experimental design and organization. Geosci Model Dev 9:1937–1958. https://doi.org/10.5194/gmd-9-1937-2016,2016

Fuentes-Franco R, Koenigk T (2019) Sensitivity of the Arctic freshwater content and transport to model resolution. Clim Dyn 53:1765–1781. https://doi.org/10.1007/s00382-019-04735-y

Ganachaud A, Wunsch C (2000) Improved estimates of global ocean circulation, heat transport and mixing from hydrographic data. Nature 408(6811):453–457. https://doi.org/10.1038/35044048

Gerber EP, Vallis GK (2009) On the zonal structure of the North Atlantic Oscillation and annular modes. J Atmos Sci 66:332–352. https://doi.org/10.1175/2008JAS2682.1

Grégorio S, Penduff T, Sérazin G, Molines JM, Barnier B, Hirschi J (2015) Intrinsic variability of the Atlantic Meridional Overturning Circulation at interannual-to-multidecadal timescales. J Phys Oceanogr 45:1929–1946. https://doi.org/10.1175/JPO-D-14-0163.1

Hawkins E, Sutton R (2007) Variability of the Atlantic thermohaline circulation described by three-dimensional empirical orthogonal functions. Clim Dyn 29:745–762. https://doi.org/10.1007/s00382-007-0263-8

Jackson LC, Kahana R, Graham T, Ringer MA, Woollings T, Mecking JV, Wood RA (2015) Global and European climate impacts of a slowdown of the AMOC in a high resolution GCM. Clim Dyn 45(11):3299–3316. https://doi.org/10.1007/s00382-015-2540-2

Jiang W, Gastineau G, Codron F (2021) Multicentennial variability driven by salinity exchanges between the Atlantic and the arctic ocean in a coupled climate model. J Adv Model Earth Syst 13:e2020MS002366. https://doi.org/10.1029/2020MS002366

Jungclaus JH, Haak H, Latif M, Mikolajewicz U (2005) Arctic–North Atlantic interactions and multidecadal variability of the meridional overturning circulation. J Clim 18(19):4013–4031. https://doi.org/10.1175/JCLI3462.1

Kanzow T, Cunningham SA, Johns WE, Hirschi JJM, Marotzke J, Baringer MO, Meinen CS, Chidichimo MP, Atkinson C, Beal LM, Bryden HL, Collins J (2010) Seasonal variability of the Atlantic Meridional overturning circulation at 26.5 degrees N. J Clim 23(21):5678–5698. https://doi.org/10.1175/2010JCLI3389.1

Knight JR, Allan RJ, Folland CK, Vellinga M, Mann ME (2005) A signature of persistent natural thermohaline circulation cycles in observed climate. Geophys Res Lett 32:L20708. https://doi.org/10.1029/2005GL024233

Laepple T, Huybers P (2013) Reconciling discrepancies between Uk37 and Mg/Ca reconstructions of Holocene marine temperature variability. Earth Planet Sci Lett 375:418–429. https://doi.org/10.1016/j.epsl.2013.06.006

Latif M, Boening CW, Willebrand J, Biastoch A, Dengg J, Keenlyside NS, Schweckendiek U, Madec G (2006) Is the thermohaline circulation changing? J Clim 19(18):4631–4637. https://doi.org/10.1175/JCLI3876.1

Latif M, Sun J, Visbeck M, Bordbar MH (2022) Natural variability has dominated Atlantic Meridional Overturning Circulation since 1900. Nat Clim Change 12:455–460. https://doi.org/10.1038/s41558-022-01342-4

Liu Z, Otto-Bliesner B, He F et al (2009) Transient simulation of last deglaciation with a new mechanism for Bølling–Allerød warming. Science 325:310–314. https://doi.org/10.1126/science.1171041

Madec G (2008) NEMO ocean engine. Technical report, Institut Pierre-Simon Laplace (IPSL)

Mann ME, Park J, Bradley RS (1995) Global interdecadal and century-scale climate oscillations during the past five centuries. Nature 378(6554):266–270. https://doi.org/10.1038/378266a0

Martin T, Park W, Latif M (2013) Multi-centennial variability controlled by Southern Ocean convection in the Kiel Climate Model. Clim Dyn 40:2005–2022. https://doi.org/10.1007/s00382-012-1586-7

McCarthy G, Haigh I, Hirschi JM, Grist JP, Smeed DA (2015) Ocean impact on decadal Atlantic climate variability revealed by sea-level observations. Nature 521:508–510. https://doi.org/10.1038/nature14491

McManus JF, Francois R, Gherardi JM, Keigwin LD, Brown-Leger S (2004) Collapse and rapid resumption of Atlantic meridional circulation linked to deglacial climate changes. Nature 428(6985):834–837. https://doi.org/10.1038/nature02494

Menary MB, Park W, Lohmann K et al (2012) A multimodel comparison of centennial Atlantic meridional overturning circulation variability. Clim Dyn 38:2377–2388. https://doi.org/10.1007/s00382-011-1172-4

Mikolajewicz U, Maier-Reimer E (1990) Internal secular variability in an ocean general circulation model. Clim Dyn 4:145–156. https://doi.org/10.1007/BF00209518

Msadek R, Frankignoul C (2009) Atlantic multidecadal oceanic variability and its influence on the atmosphere in a climate model. Clim Dyn 33:45–62. https://doi.org/10.1007/s00382-008-0452-0

Oppo D, McManus J, Cullen J (2003) Deepwater variability in the Holocene epoch. Nature 422:277. https://doi.org/10.1038/422277b

Rahmstorf S (2002) Ocean circulation and climate during the past 120,000 years. Nature 419(6903):207–214. https://doi.org/10.1038/nature01090

Roquet F, Madec G, McDougall TJ, Barker PM (2015) Accurate polynomial expressions for the density and specific volume of seawater using the TEOS-10 standard. Ocean Model 90:29–43. https://doi.org/10.1016/j.ocemod.2015.04.002

Serreze MC, Barrett AP, Slater AG, Woodgate RA, Aagaard K, Lammers RB, Steele M, Moritz R, Meredith M, Lee CM (2006) The large-scale freshwater cycle of the Arctic. J Geophys Res 111:C11010. https://doi.org/10.1029/2005JC003424

Steinman BA, Mann ME, Miller SK (2015) Atlantic and Pacific multidecadal oscillations and Northern Hemisphere temperatures. Science 347:988–991. https://doi.org/10.1126/science.1257856

Sutton RT, Dong B (2012) Atlantic Ocean influence on a shift in European climate in the 1990s. Nat Geosci 5:788–792. https://doi.org/10.1038/ngeo1595

Valcke S (2013) The OASIS3 coupler: a European climate modelling community software. Geosci Model Dev 6:373–388. https://doi.org/10.5194/gmd-6-373-2013

Vancoppenolle M, Bouillon S, Fichefet T, Goosse H, Lecomte O, Morales Maqueda M, Madec G (2012) LIM, The Louvain-la-Neuve sea ice model, Notes du Pôle de modélisation

Vellinga M, Wu P (2004) Low-latitude freshwater influence on centennial variability of the Atlantic thermohaline circulation. J Clim 17(23):4498–4511. https://doi.org/10.1175/3219.1

Weijer W, Cheng W, Garuba OA, Hu A, Nadiga BT (2020) CMIP6 models predict significant 21st century decline of the Atlantic Meridional Overturning Circulation. Geophys Res Lett. https://doi.org/10.1029/2019GL086075

Xu X, Hurlburt HE, Schmitz WJ, Zantopp RJ, Fischer J, Hogan PJ (2013) On the currents and transports connected with the Atlantic meridional overturning circulation in the subpolar North Atlantic. J Geophys Res Oceans 118:502–516. https://doi.org/10.1002/jgrc.20065

Xu X, Chassignet EP, Johns WE, Schmitz WJ, Metzger EJ (2014) Intra-seasonal to interannual variability of the Atlantic meridional overturning circulation from eddy-resolving simulations and observations. J Geophys Res Oceans 119:5140–5159. https://doi.org/10.1002/2014JC009994

Yang J (2015) Local and remote wind stress forcing of the seasonal variability of the Atlantic Meridional Overturning Circulation (AMOC) transport at 26.5° N. J Geophys Res Oceans 120(4):2488–2503. https://doi.org/10.1002/2014JC010317

Zhang R, Delworth TL (2005) Simulated tropical response to a substantial weakening of the Atlantic thermohaline circulation. J Clim 18(12):1853–1860. https://doi.org/10.1175/JCLI3460.1

Zhang R, Delworth TL, Held IM (2007) Can the Atlantic Ocean drive the observed multidecadal variability in Northern Hemisphere mean temperature? Geophys Res Lett 34:L02709. https://doi.org/10.1029/2006GL028683

Zhao J, Johns WE (2014) Wind-forced interannual variability of the Atlantic meridional overturning circulation at 26.5°N. J Geophys Res Oceans 119:2403–2419. https://doi.org/10.1002/2013JC009407